

RSC Advances



This is an *Accepted Manuscript*, which has been through the Royal Society of Chemistry peer review process and has been accepted for publication.

Accepted Manuscripts are published online shortly after acceptance, before technical editing, formatting and proof reading. Using this free service, authors can make their results available to the community, in citable form, before we publish the edited article. This *Accepted Manuscript* will be replaced by the edited, formatted and paginated article as soon as this is available.

You can find more information about *Accepted Manuscripts* in the [Information for Authors](#).

Please note that technical editing may introduce minor changes to the text and/or graphics, which may alter content. The journal's standard [Terms & Conditions](#) and the [Ethical guidelines](#) still apply. In no event shall the Royal Society of Chemistry be held responsible for any errors or omissions in this *Accepted Manuscript* or any consequences arising from the use of any information it contains.

Multifactorial evaluation of the electrochemical response of a microbial fuel cell

Cite this: DOI: 10.1039/x0xx00000x

G. Lepage^{a,c}, G. Perrier^{a,*}, G. Merlin^a, N. Aryal^{b,d}, X. Dominguez-Benetton^{b,*}

Received 00th January 2012,
Accepted 00th January 2012

DOI: 10.1039/x0xx00000x

www.rsc.org/

A lab-scale microbial fuel cell (MFC) with reticulated vitreous carbon (RVC) anode and non-catalyzed multi-layered carbon air-cathode was electrochemically characterized under various physicochemical factors: temperature (15-25 °C), phosphate buffer concentration (4-8 mM), acetate concentration (7.1-14.3 mM), and equivalent solution conductivity (2.5-5 mS.cm⁻¹). A fundamental step was undertaken to identify and characterize the electrochemical mechanisms through multifactorial evaluation of the simultaneous effect of such factors on the functioning of the MFC. This type of analysis over cyclic voltammetry and impedance spectroscopy parameters revealed complementary features to model the electrochemical response. This multifactorial approach finds broad application in wide variety of MFC and environmental technology studies.

Introduction

Microbial electrochemical technologies (METs) are defined as systems in which microbes work as electrocatalysts. This principle applied to the conversion of organic matter into electricity led to the concept of microbial fuel cells (MFCs). In order to make MFCs suitable for practical applications, a better understanding of the effects of reactor design and operation mode on power densities is required¹. Optimization of operational conditions (e.g. pH, temperature, organic load, feed rate, and shear stress) is essential for the development of MFCs, because their performance is still far below ideal².

The development of MFCs should then meet the following issues: What intensification strategies can be implemented to optimize chemical and energy conversion efficiencies? How to characterize and control the mechanistic phenomena inherent to microbial-electrochemical reactions at each electrode? The issue of reactor engineering focuses largely on optimizing the transfer of matter and energy within the system. MFC voltages always appear lower than ideal values due to three types of irreversible losses occurring within the system: activation polarization, ohmic losses and concentration polarization². At the biofilm level, mass and energy transfer interfaces are constrained, and absorption of the substrate is the limiting phenomenon for the overall kinetics prior to the external electron transfer³. When the biofilm and its aqueous medium present a low thickness, the surface current density can be particularly high⁴. The mechanisms governing adhesion processes, development and detachment of biofilms in aqueous media in relation to the substrate characteristics (porosity, roughness, hydrophobicity, charge, pH, surface potential) have

been largely studied^{5,6,7}, as well as the influence of the independent physicochemical conditions⁸ and flow regime⁹. Nevertheless, to our best knowledge, no studies have specifically described the sensitivity of electrochemically active biofilms on simultaneously tested factors.

This research aimed to evaluate the combined effect of four key physicochemical operating parameters (temperature, buffer capacity, acetate concentration and conductivity) on the electrochemical activity of a single chamber air-cathode MFC. Air-cathode MFCs are advantageous due to simplified reactor configuration as well as high power output as compared to double-chamber MFCs. Reticulated Vitreous Carbon (RVC) was selected as the anode material due to previous proof of good stability and fair robustness¹⁰. This material offers the advantage of presenting modular macro porosities (4-40 pores.cm⁻¹), very high permeability (up to 97% open porosity) and an isotropic macroscopic structure. Specific surface area ranges from 800 to 6800 m².m⁻³, depending on porosity¹¹. The multifactorial experimental plan selected to conduct this study provides a quick access to the main factors interactions and can be straightforwardly extended to a wide variety of MFC studies.

Experimental

MFC construction

A 32-cm³ single-chamber MFC (Figure 1a) was constructed out of polymethylmethacrylate (PMMA). The anode consisted of a 2×2×0.32 cm³ piece of RVC (*Goodfellow*; 24 pores per cm; 48 cm² of active surface area), connected to a stainless steel screw and titanium wire as current collector (Figure 1b). No specific pre-treatment was carried out on the material prior to

inoculation. The air-cathode consisted of a specially designed multilayer assembly as presented in Figure 1c (*Paxitech, Grenoble, F*; $4 \times 4 \text{ cm}^2$). This non-platinized assembly uses a stainless steel grid for mechanical rigidity and electrical connection, together with the carbon felt. The material in contact with the electrolyte consisted in a carbon powder-PTFE composite. The carbon microporous layers allow the penetration of oxygen, and the external PTFE layer is a good compromise between oxygen transfer and water evaporation¹². The air-cathode is separated from the anodic compartment by a Dupont Nafion® N-117 cation exchange membrane (*Ion Power*; 16 cm^2) which was held onto the active surface of the air-cathode by a plastic mesh. Prior to installation, the membrane was pre-treated by immersion in H_2O_2 3% v/v at 110°C for 1 h, then 1 M HNO_3 for 1 h, and subsequently rinsed in deionized water. The reference electrode was an Ag/AgCl (+199 mV/SHE) and a 1 k Ω external resistor was connected between anode and cathode.

MFC operation

The MFC reactor was first inoculated with a biomass mix originated from an activated sludge from the local wastewater treatment plant (Le Bourget du Lac, France) and a previously operating MFC anodic suspension. 10 mL of the obtained inoculum were diluted in 15 mL of a buffered nutrient solution containing 8 mM Na_2HPO_4 , 2 mM NH_4Cl , 14 mM $\text{CH}_3\text{CO}_2\text{Na}$ and 0.05 g.L^{-1} yeast extract. pH and conductivity were adjusted at 7.0 and 5.0 mS.cm^{-1} , respectively. The system was conducted at 25°C under a 1 k Ω external resistance during the first 4 weeks of operation, until the cell reached a stable and reproducible power output of 5.2 mW.m^{-2} (0.11 V; 48 mA.m^{-2} ; measured to the cathode projected surface area). Once exhausted, the electrolyte was replaced weekly by 25 mL of fresh broth. After the starting phase, the MFC was operated in 8 different combinations of temperature, phosphate buffer concentration, acetate concentration and conductivity, to assess the effect of these factors and their interactions on: a) current-voltage, b) time- and c) frequency-domain impedance responses of the cell.

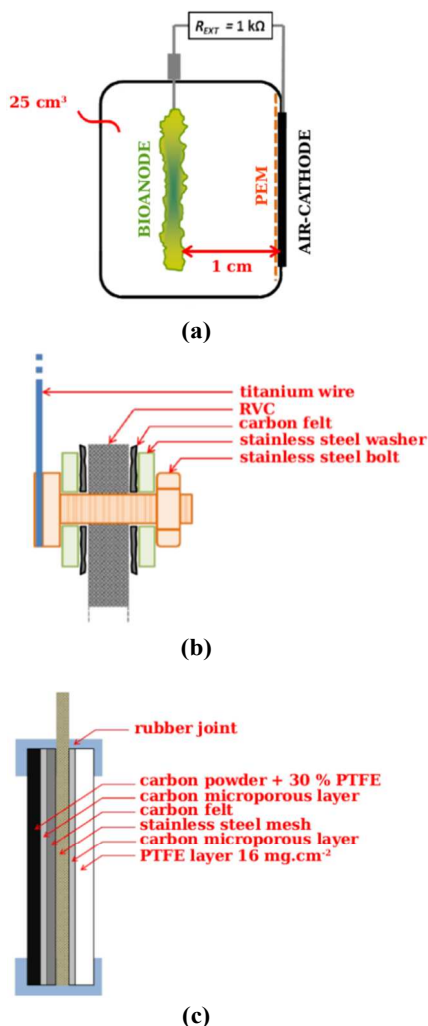


Figure 1: Schematic representations of: (a) single-chamber air-cathode MFC; (b) RVC anode-to-current collector connection; (c) air-cathode multilayer configuration.

Electrochemical measurements

The electrochemical response of the cell was measured in steps: (1) The anolyte was renewed with a 25 mL fresh broth and the MFC cell voltage was let to stabilize overnight ($\sim 15 \text{ h}$) under the 1 k Ω external resistance ($E_{CELL-1k\Omega}$). Cell voltage was recorded every 5 min. (2) A cyclic voltammetry scan of the anode was performed relatively to the reference electrode. The anodic potential was first stabilized at $+0.23 \text{ V/SHE}$ for 300 s, then scanned at 0.5 mV.s^{-1} down to -0.37 V/SHE and back to $+0.23 \text{ V/SHE}$, in order to determine the maximum anodic current density (j_L) as illustrated in Figure 2 for a typical experiment. (3) To obtain the polarization and power density curves of the cell, the cell voltage between anode and cathode was set to short-circuit conditions during 300 s, then down to open-circuit conditions at a scan rate of 0.5 mV.s^{-1} (see Figure 3 for a typical experiment), allowing determination of cell maximum power (P_{MAX}), short-circuit current density (J_{sc}) and internal resistance (R_{INT}). (4) The current flow between anode and cathode was forced to 0 A during 3 h (open-circuit), to determine anodic and cathodic open-circuit potentials (E_{OCPA} and E_{OCPC}) measured to the reference electrode. (5) The circuit was closed for 1 h to ensure stable biofilm electrochemical activity. (6) To determine the cell impedance, a 30 mV AC potential was overimposed to E_{OCPA} , E_{OCPC} , and the open circuit potential of the cell, respectively. This excitation signal was applied at 30 different frequencies ranging from 100 kHz to 5 mHz to obtain the impedance spectra of the cell for different electron transport regimes. For low frequency measurements ($< 3 \text{ kHz}$), the multisine option of the frequency response analyzer was used in order to increase the acquisition speed. This option allows creating a frequency scan in which low frequency single sines are replaced by a linear combination of five harmonics. Each multisine signal thus generated five data points, so each recorded spectrum contains 141 data points.

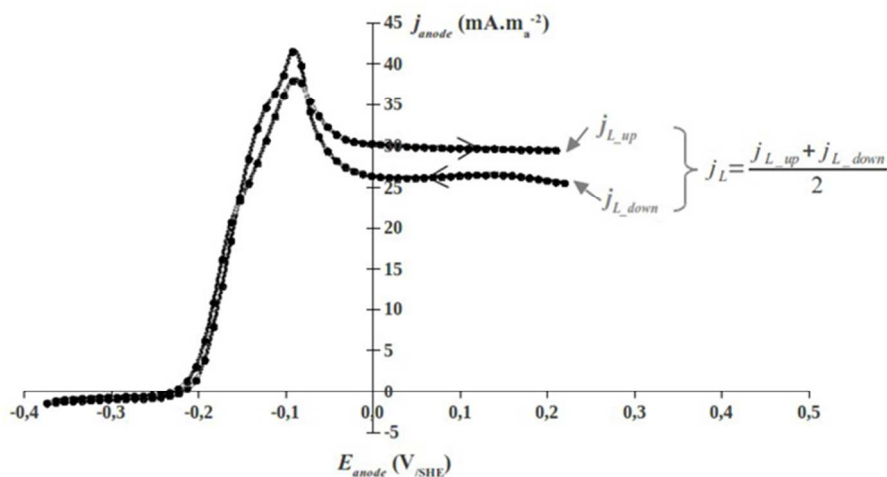


Figure 2: Typical cyclic voltamogram (here for combination 6) showing the measurement of the maximum anodic current density J_L (measured to the anode area).

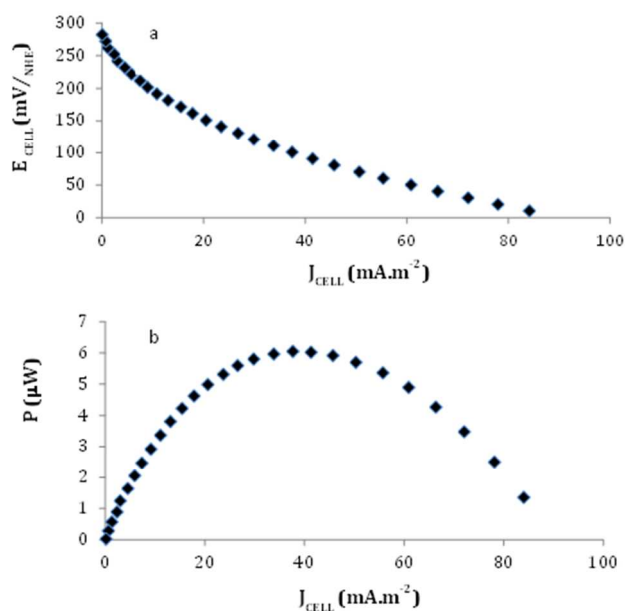


Figure 3: Typical polarization (a) and power (b) curves (here for combination 6).

Validity of impedance data and calculations

The validity of impedance data was tested relatively to the four usually accepted criteria that are linearity, causality, stability and finiteness^{13,14}. Especially, the stability condition was verified by application of the Kramers-Kronig transform^{15,16} using EC-Lab v.10.2, with data imported as text files. Data consistency was assessed by inspection of the successful regression (correlation coefficient $R^2 > 0.99$) to experimental data, with several electrical analogues composed of Voigt elements. Impedance data were analyzed as explained by Dominguez-Benetton *et al.*¹⁴: (a) the obtained impedance spectra were plotted in the $-Z_{im}$ versus frequency representation (logarithmic scale); (b) by calculation of the first derivative of

this plot, the relative maxima of the function were determined; (c) the algebraic slope of the curves above the relaxation frequency was determined¹⁷ and magnitudes consistent with distributed electrical parameters were obtained in all cases.

The absolute magnitudes of the slopes were directly attributed to the Constant Phase Element (CPE) parameter α , as defined in the CPE impedance response:

$$Z_{CPE} = 1/Q(j\omega)^\alpha \quad (1)$$

Here, j is the imaginary unit ($j^2 = -1$) and ω is the angular frequency ($\omega = 2\pi f$, f being the frequency in Hz). The CPE parameters Q and α are frequency-independent constants; Q represents the differential capacitance of the interface. The

dimensionless parameter α can be related to the angle of rotation relatively to a purely capacitive line on the complex plane plots. The pseudo-capacitive CPE parameter Q was thus calculated according to Equation 2:

$$Q = -\sin(\alpha\pi/2)/Z_{im}\omega^\alpha \quad (2)$$

where the ω and Z_{im} magnitudes corresponded to those evaluated at the relative maximum corresponding to the time constant (R_iC_i) in question.

Effective capacitance

The EIS response can be explained by the use of deterministic models which propose information concerning processes at the interface of an electrochemical system. Such processes include thermodynamic and kinetic information, as well as intrinsic physico-chemical properties such as permittivity and conductivity^{18,19}.

An artifact that is commonly used to model EIS data of heterogeneous interfaces, such as those developed in porous electrodes, is the CPE. Z_{CPE} represents the response of a pure capacitor when $\alpha = 1$. In the same way, Z_{CPE} behaves as a pure resistor when $\alpha = 0$. However, many electrochemical systems behave differently; when $0 < \alpha < 1$, Z_{CPE} cannot represent the response of either a pure capacitance or resistance¹⁸. For this reason, the CPE is used as a quite flexible mathematical parameter for fitting impedance data. The existence of a CPE in the EIS response model of an electrochemical interface can be justified from the magnitude of the slope of the curve obtained in the imaginary part of the impedance plotted with respect to frequency in a logarithmic scale¹⁷. However, the physical meaning of a process underlying such a response cannot be clarified from just the purely mathematical description that a CPE model represents^{19,14}.

The physical origins of the CPE are controversial. CPE parameters are thought to arise from a distribution of time-constants, two types of them being commonly considered: normal and surface distributions. The distribution of these time-constants results from the distributions of physical properties including structure, reactivity, dielectric constants, and resistivity. A normalized probability distribution of time constants can be anticipated in systems involving dielectric or conductive dispersion, such as oxide films, organic coatings, as well as human skin, cell membrane and systems with distributed porosity or surface-roughness such as microbial electrodes¹⁴. Conversely, for other materials, the surface-dispersed properties cannot result in a normalized probability function. In the latter systems, the local ohmic resistance, which is surface-distributed, significantly contributes to the impedance response. An example of this type of geometry-dependent distribution has been suggested for the ideally polarized blocking electrode¹⁸. In the case of the present work, highly porous carbon-based materials were used as both substrates for the development of the anodic electrochemically-active biofilm and for the air-cathode.

Therefore, a normal-distribution of the physical properties of the interfaces is anticipated.

Several models can be used to extract relevant parameters from CPE data. Specifically, the effective capacitance is used to resolve charge accumulation. The pseudo-capacitive CPE parameter Q is thus calculated from the graphically obtained slope α , as per Equation 2. Following the power-law model for distribution of local resistivity with a uniform dielectric constant¹⁸, the effective capacitance can be calculated:

$$C_{eff} = gQ(\rho_0\epsilon\epsilon_0^{1-\alpha}) \quad (3)$$

ϵ being the dielectric constant, ϵ_0 the permittivity of vacuum (8.8542×10^{-14} F.cm⁻¹), ρ_0 the boundary value of resistivity at the interface, and g a numerically-evaluated function:

$$g = 1 + 2.88(1 - \alpha) 2.375 \quad (4)$$

Quantitative and qualitative analysis of C_{eff} , Z_{im} and α , together with supplementary information provided by distinct characterization methods and supplementary modeling can provide key information about the phenomena and mechanisms taking place at the electrode-electrolyte interface. For this reason, these parameters were here taken into account.

Multifactorial experimental plan

Four physicochemical factors (temperature, phosphate buffer concentration, initial acetate concentration and conductivity at 25 °C) were tested. Two levels were chosen for each factor, within ranges that are typical for real domestic or industrial sewage MFC operations: 15 and 25 °C for temperature, 4 and 8 mM for phosphate buffer concentration, 7.1 and 14.3 mM (corresponding to 0.4 and 0.8 g_{COD}.L⁻¹, respectively) for initial acetate concentration, and 2.5 and 5.0 mS.cm⁻¹ for conductivity. The pH was adjusted to 7.0, and 0.1 g.L⁻¹ of NH₄Cl were added as nitrogen source for bacteria. Based on the Taguchi statistical method, an orthogonal experimental plan was constructed with eight combinations (*i.e.* eight assays), in order to study interactions between the selected factors (Table 1).

Table 1: Multifactorial experimental plan with i being the label of the combination.

| i | T (°C) | [buffer] (mM) | [acetate] (mM) | σ (mS.cm ⁻¹) |
|-----|--------|---------------|----------------|---------------------------------|
| 1 | 15 | 4.0 | 7.1 | 2.5 |
| 2 | 15 | 4.0 | 14.3 | 5.0 |
| 3 | 15 | 8.0 | 7.1 | 5.0 |
| 4 | 15 | 8.0 | 14.3 | 2.5 |
| 5 | 25 | 4.0 | 14.3 | 5.0 |
| 6 | 25 | 4.0 | 7.1 | 2.5 |
| 7 | 25 | 8.0 | 14.3 | 2.5 |
| 8 | 25 | 8.0 | 7.1 | 5.0 |

Results and discussion

Effect of factors on the electrochemical response

The eight combinations of the experimental plan were tested according to the order presented in Table 1. As the measurement process took one day for each combination, the whole experimental plan was completed approximately within a

week. Additionally, cyclic voltammetry measurements were repeated for combinations 2, 1, 5 and 7 during the following week to ensure no significant signal deviations (*i.e.* < 5 %). Table 2 summarizes the resulting measured MFC electrochemical parameters, in terms of various voltages and currents densities, power and internal resistance.

Table 2: Electrochemical responses obtained for the eight combinations of the experimental plan. Voltages for anode and cathode are expressed relative to SHE; j_L and J_{sc} current densities refer to the anode and the cathode, respectively.

| i | $E_{CELL-1k\Omega}$ (mV) | E_{OCPA} (mV/SHE) | E_{OCPC} (mV/SHE) | j_L (mA.m ⁻²) | J_{sc} (mA.m ⁻²) | P_{MAX} (mW.m ⁻²) | R_{INT} (Ω) |
|------|-----------------------------|------------------------|------------------------|--------------------------------|-----------------------------------|------------------------------------|---------------------------|
| 1 | 47.7 ± 2.0 | -210 ± 5 | 210 ± 5 | 12.6 ± 0.0 | 36.3 ± 0.2 | 2.87 ± 0.02 | 3350 ± 190 |
| 2 | 51.2 ± 2.0 | -210 ± 5 | 210 ± 5 | 11.1 ± 0.0 | 36.3 ± 0.7 | 3.46 ± 0.03 | 3200 ± 110 |
| 3 | 52.7 ± 2.0 | -220 ± 5 | 220 ± 5 | 12.0 ± 0.5 | 39.4 ± 0.6 | 4.20 ± 0.03 | 3090 ± 50 |
| 4 | 47.9 ± 2.0 | -220 ± 5 | 220 ± 5 | 11.1 ± 0.0 | 32.5 ± 1.2 | 3.14 ± 0.03 | 4100 ± 460 |
| 5 | 109.8 ± 2.0 | -270 ± 5 | 190 ± 5 | 19.2 ± 0.4 | 90.6 ± 5.3 | 6.64 ± 0.05 | 1440 ± 20 |
| 6 | 98.7 ± 2.0 | -270 ± 5 | 180 ± 5 | 31.6 ± 1.8 | 90.6 ± 7.1 | 6.04 ± 0.05 | 1150 ± 10 |
| 7 | 94.2 ± 2.0 | -270 ± 5 | 180 ± 5 | 20.3 ± 0.9 | 75.0 ± 2.5 | 5.75 ± 0.05 | 1760 ± 80 |
| 8 | 104.3 ± 2.0 | -270 ± 5 | 190 ± 5 | 22.6 ± 1.3 | 93.8 ± 6.4 | 6.15 ± 0.05 | 1230 ± 10 |
| mean | 75.8 ± 2.0 | -243 ± 5 | 200 ± 5 | 17.6 ± 0.7 | 61.8 ± 3.0 | 4.78 ± 0.04 | 2415 ± 120 |

For each response R , the absolute effect $\Delta_{F,R}$ and unit effect $\Delta'_{F,R}$ (the effect normalized to its unit) of each factor F were calculated as stated by equations 5 and 6, L_1 and L_2 being the two levels for each factor.

$$\Delta_{F,R} = R_{F,L2} - R_{F,L1} \quad (5)$$

$$\Delta'_{F,R} = (R_{F,L2} - R_{F,L1}) / (L_2 - L_1) \quad (6)$$

$\Delta_{F,R}$ and $\Delta'_{F,R}$ results are presented in Table 3. Only significant effects (*i.e.* effects over measurement uncertainty) are retained. A positive effect is considered when $E_{CELL-1k\Omega}$, E_{OCPC} , j_L , J_{sc} and P_{MAX} significantly increase when the factor value increases, or when E_{OCPA} and R_{INT} significantly decrease when the factor value increases.

Table 3: Absolute ($\Delta_{F,R}$) and unit ($\Delta'_{F,R}$) effects of the four selected factors on the electrochemical response of the MFC. Only effects greater than measurement uncertainty are retained.

| | $E_{CELL-1k\Omega}$ (mV) | E_{OCPA} (mV/SHE) | E_{OCPC} (mV/SHE) | j_L (mA.m ⁻²) | J_{sc} (mA.m ⁻²) | P_{MAX} (mW.m ⁻²) | R_{INT} (Ω) |
|---|-----------------------------|------------------------|------------------------|--------------------------------|-----------------------------------|------------------------------------|---------------------------|
| $\Delta_{F,R}$ | | | | | | | |
| Δ_T | +51.9 | -55 | -30 | +11.8 | +51.4 | +2.7 | -2040 |
| $\Delta_{[buffer]}$ | +2.9 | | | +1.8 | | +0.4 | |
| $\Delta_{[acetate]}$ | | | | -4.3 | -6.4 | -0.07 | +420 |
| Δ_σ | +7.4 | | | -2.7 | +6.4 | +0.66 | -350 |
| $\Delta'_{F,R}$ | | | | | | | |
| Δ'_T (for 1 °C) | +5.2 | -5.5 | -3.0 | +1.2 | +5.1 | +0.3 | -204 |
| $\Delta'_{[buffer]}$ (for 1 mM) | | | | | | +0.1 | |
| $\Delta'_{[acetate]}$ (for 1 mM) | | | | -0.7 | | | |
| Δ'_σ (for 1 mS.cm ⁻¹) | +3.0 | | | -1.1 | | +0.3 | -140 |

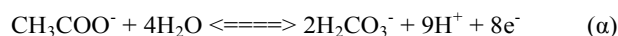
Effect of temperature. Table 3 shows a high sensibility of the system to the temperature factor. Except for E_{OCPC} , a temperature change as low as 1 °C (normalized unit) is seen to have a significant positive effect. In a first approximation one can consider that +1 °C in temperature in the range 15-25 °C increases j_L , J_{sc} and P_{MAX} by 6-8 % for our system. The apparent Q_{10} temperature coefficient, defined as:

$$Q_{10} = (R_2/R_1)^{10(T_2 - T_1)} \quad (7)$$

where R are the responses and T the temperatures, is close to 2 for these three parameters, which is consistent with a kinetic-dependent behavior as it has been shown that a 10 °C rise in temperature increases the rate of a biochemical reaction by about 1.5 to 2.5 times²⁰. In the work of Gonzalez del Campo *et al.*²¹, the calculated temperature coefficient was 1.12, indicating that an increase of 10 °C caused a 12 % increase in the intensity generated by the MFC. Thus, in the present case, an improvement of the system has to go through strategies

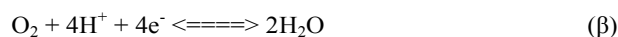
focusing on kinetic limitations. Nevertheless, because of the fact that conductivity is also dependent on the temperature, the positive effect of temperature is seen to be mainly a combined action of the temperature on reaction rates with the actual electrolyte conductivity changes. As a result, the strong effect of an increase in temperature on the reactor internal resistance R_{INT} is doubtless primarily linked to an increase in conductivity of the electrolyte and membrane²², which significantly decreases the ohmic resistance. For example, the internal resistance of the MFC is shown to decrease by approximately 0.6 % per °C as reported by Gonzalez del Campo *et al.*²¹.

The anode and cathode open-circuit potentials E_{OCPA} and E_{OCPC} are negatively affected by temperature (respectively 55 and 30 mV between 15 and 25 °C). Such a phenomenon is predicted by thermodynamics in Nernst equations (equations 8 and 9) applied to anodic (α) and cathodic reactions (β):



$$E_{anode}^0 = E_{acetate}^0 + (RT/nF) \ln \left(\frac{[\text{H}_2\text{CO}_3]^2 [\text{H}^+]^9}{[\text{CH}_3\text{COO}^-]} \right) \\ = 0.187 + 1.077 \times 10^{-5} \times T \times \ln(0.1 \times 10^{-9pH}) \quad (8)$$

The concentration ratio between $[\text{H}_2\text{CO}_3]^2$ and $[\text{CH}_3\text{COO}^-]$ is set to 0.1, reflecting the reaction stationary state.



$$E_{cathode}^0 = E_{\text{H}_2\text{O}}^0 + (RT/nF) \ln(p\text{O}_2 [\text{H}^+]^4) \\ = 1.223 + 2.154 \times 10^{-5} \times T \times \ln(0.21 \times 10^{-4pH}) \quad (9)$$

where $p\text{O}_2 = 0.21$ is the oxygen partial pressure in air.

According to Equation 8, the anodic nernstian potential should decrease with temperature. An open-circuit potential drop of 55 mV was measured between 15 and 25 °C, at pH 7, whereas only 16 mV are expected from theoretical calculations due to the 10 °C temperature increase (-0.270 V/SHE vs. -0.286 V/SHE, respectively). This can imply that the temperature raise can also affect mass transfer by increasing molecular diffusion, according to Arrhenius law.

For its part, Equation 9 predicts a cathodic potential drop of -14 mV between 15 and 25 °C, relatively to the 10 °C temperature increase (+0.813 V/SHE vs. +0.799 V/SHE, respectively) at pH 7. This drop is strongly dependent on the pH magnitude. For instance, the cathodic nernstian potential drop is -30 mV between pH 7 and pH 12 at 25 °C. Such alkaline conditions at cathodes surfaces (pH > 12) have already been reported in MFC with Nafion-based separators, due to the limiting capacity of the membrane to supply protons for the cathodic reaction^{23,24}. A more alkaline pH at the air-cathode liquid interface in the present cell may explain the -14 mV loss here observed.

Effect of buffer concentration. Increasing the concentration of electrolyte buffer by 1 mM (normalized unit) in the range 4-8 mM produces little effect on the MFC performance. No bulk variation in pH was noticed during a whole batch period (~7 days), even at low buffer concentration. Although a variation on buffer concentration as small as 1 mM has no significant effect, a larger increase of 4 mM has a more noticeable positive effect on $E_{CELL-1K\Omega}$, j_L and P_{MAX} . Torres *et al.*²⁵ showed that

maximum current generation was directly related to transport of phosphate buffer by diffusion inwards and outwards the biofilm. Even in the case of a well-controlled pH by buffer addition, the chemical nature of the buffer largely impacts on power production, even at identical concentrations, due to their inherent electrolyte conductivities²⁶. The phosphate buffer, having a pK_a close to neutral pH, maximizes the increase in current generation. Considering the buffer concentration used here, the system lies an order of magnitude lower than synthetic media usually used as anolyte in MFC. Such a buffer concentration (> 50 mM) is inconsistent with real wastewaters, except for some particular industrial sewages. Still, doubling the buffer concentration from 4 to 8 mM is equivalent to an addition of 600 g.m⁻³ of disodium phosphate, which is neither economically nor environmentally relevant.

Effect of substrate concentration. A variation of ± 1 mM in the range 7.1-14.3 mM has nearly no effect on the MFC response. The only parameter affected is j_L , which decreases by ~6 % when COD increases by 1 mM. This may point out a kind of inhibitory effect caused by an excess of substrate on metabolic pathways. Unlike methanogens, anode-respiring bacteria are able to efficiently deal with diluted effluents.

Effect of electrolyte conductivity. When the conductivity increases by 1 mS.cm⁻¹ in the range 2.5-5 mS.cm⁻¹, a positive effect of about 4-6 % on $E_{CELL-1K\Omega}$, P_{MAX} and R_{INT} is noticed. Higher conductivities enhance the ionic mobility that determines internal ohmic losses, thus the reactor internal resistance and maximal power²⁷. Conversely, the negative effect of an increase of conductivity on j_L (-6.3 % per mS.cm⁻¹) may mislead the fact that the biofilm activity is sensitive to high ionic strength.

Effect of factors on impedance response

For the eight combinations of the experimental plan, the respective anode and cathode interfacial impedances were measured, as well as the whole cell impedance, at various excitation frequencies. A selection of spectra for the first 3 combinations is presented in Figures 4 (complex Nyquist domain) and 5 (Bode plot, phase angle).

Prior to the establishment of equivalent circuit models, a thoughtful analysis of the pseudo-time constants was carried out for each interface (anode and cathode) and for the whole cell, as per the explanation provided for validity of EIS data and calculations. For consistency purposes, EIS data are only analyzed from 1.709 kHz to 5 mHz. Although values at higher frequencies were recorded, such could not be validated, as they may introduce the effect of parasitic inductances. From the $-Z_{im}$ versus frequency representation on a logarithmic scale, the algebraic slopes α above each relaxation frequency were determined. In all cases, magnitudes consistent with distributed electrical parameters were obtained (see a CPE type of behavior). The pseudo-capacitive contributions Q were calculated for each slope through Equation 2. The electrolyte resistance was determined by interpolation of the EIS response to the abscissa axis (where $-Z_{im} = 0$); this parameter was validated with conductivity measurements.

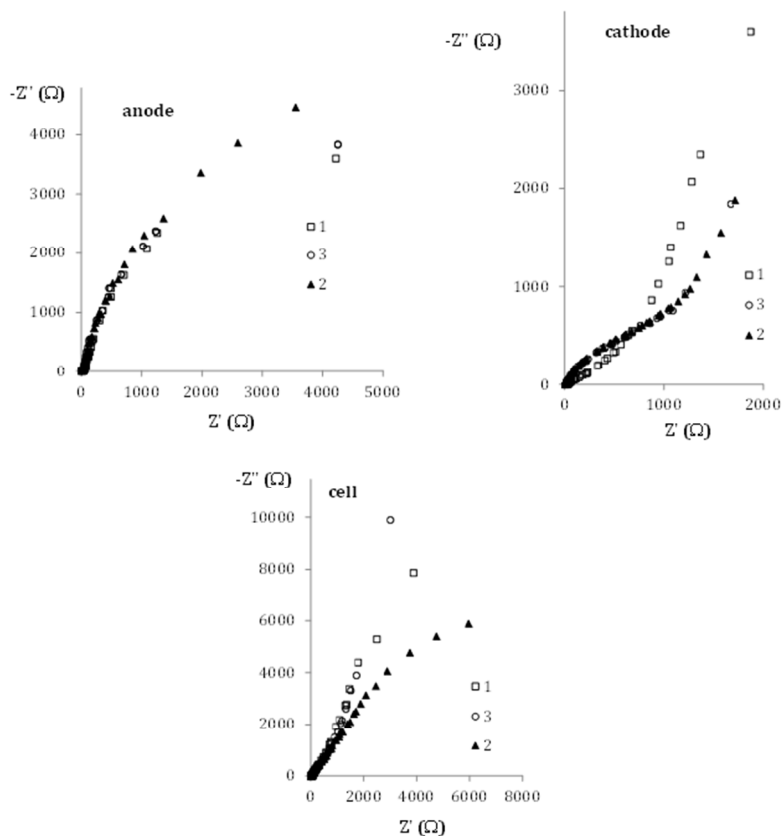


Figure 4: Nyquist impedance spectra for the anode, the cathode and the entire cell for the first three combinations tested.

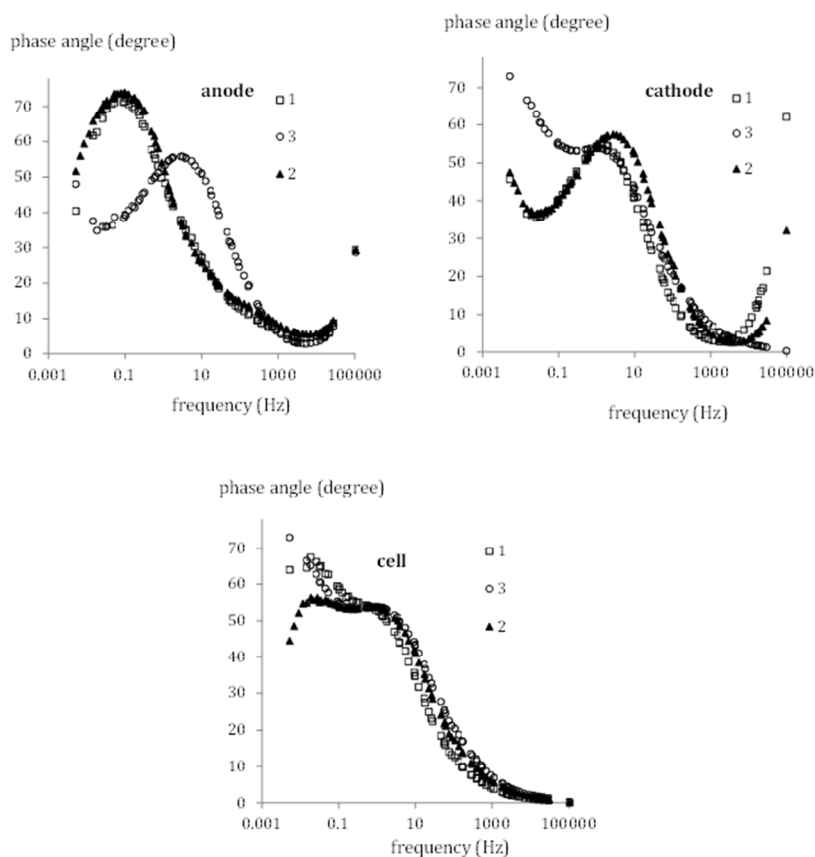


Figure 5: Bode impedance spectra for the anode, the cathode and the entire cell for the first three combinations tested.

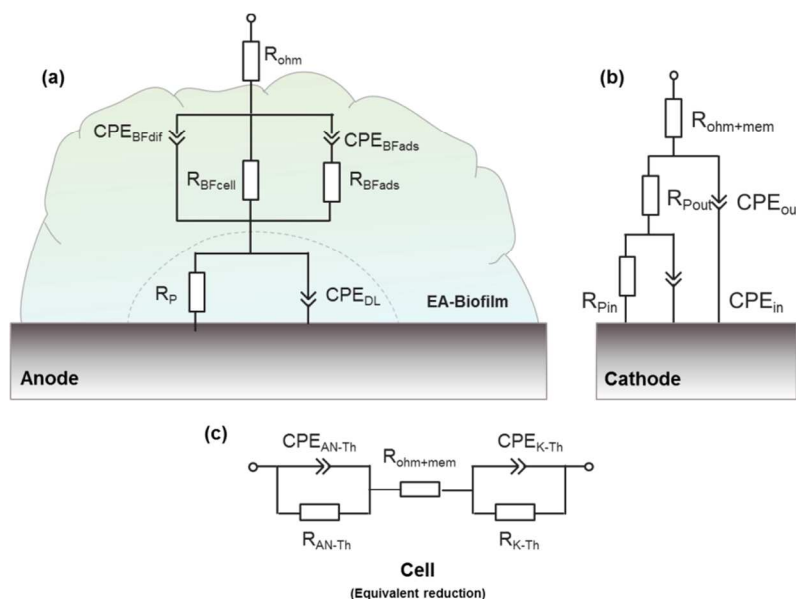


Figure 6: Electrical equivalent circuit models for: (a) anode, (b) cathode, and (c) whole cell as proposed by the Thévenin AC circuit reduction of (a) and (b). Resistances R and constant phase elements CPE are relevant to the corresponding physics of the electrochemical interfaces. Ohm: ohmic; BF: biofilm; dif: contribution to diffusional limitations; ads: contribution to adsorption limitations; P; polarization; DL: double layer; Pout: polarization due to the outer porous structure; Pin: polarization due to the inner porous structure; mem: ion exchange membrane; AN: anode; K: cathode; Th: Thévenin simplification.

With such equivalent electrical parameters, equivalent circuit models were finally proposed, without any free parameter¹⁴. Circuits relevant to the nature of the electrochemical processes taking place for each case (anode, cathode and whole cell) were proposed for every experimental combination (Figure 6). For the case of the full cell system, a simple addition of the anodic and cathodic contributions is possible, perfectly describing the overall impedance behavior. However, due to some pseudo-time constants being partially masked by the overlapping contributions of the anode and the cathode, and thus the number of points corresponding to a unique slope being somewhat ambiguous, it was proposed to consider a simplified case holding comparable statistical deviation. The descriptive simplification was carried out using the Thévenin theorem for linear AC electrical impedance networks using a voltage source (Figure 6c). The simplex linear regression method was computed using EC-Lab (with 10000 iterations) to optimize parameters estimations. The minimal standard deviations (σ) for each parameter were targeted as descriptors of insignificant dispersion from model with respect to experimental data. An arbitrary limit of $\sigma = 0.05$ was set to ensure above 95 % confidence interval for at least 98 % of the data recorded in a single EIS spectrum.

Table 4 presents the values of the various equivalent circuit parameters obtained for the anode, cathode and whole cell, and optimized with the EC-Lab software, for each tested combination. Resistors are characterized by their resistance R and Constant Phase Elements by their pseudo-capacitance Q and adjustment factor α as stated in Equation 1. In the case of R_{Pin} for combinations 1 and 3, and R_{AN-Th} for combination 3, the

unreliable calculated values were replaced by the observed mean value (bold case). Some interesting features can be extracted from this table. The series resistances for both anode and cathode are in the range 10-20 Ω , validating the suitability of the design and construction of the MFC in terms of electrical connections, size and global electrolyte and membrane resistivities. In the case of the cathode and whole cell, the series resistances include the contribution of the Nafion® membrane, the resistance of which do not seem to be detrimental to the global reactor resistance. The series resistance of the whole cell is as expected of the order of the sum of the series resistances for separately considered anode and cathode. For their part, the values of the α parameters are spread over a large range (0.36-0.93), showing the very large kinds of physical characteristics for the pseudo-capacitances in the electrical equivalent circuits (polarization, diffusion and adsorption phenomena, presence of a biofilm). As per the α magnitudes, it is inferred that heterogeneity of the distributed properties at whole cell level is due to adsorption phenomena at the electrochemically active biofilm interface.

Although all values roughly lie in the ranges 10-1000 Ω for resistances and 0.1-10 $\text{mF}\cdot\text{s}^{(\alpha-1)}$ for pseudo-capacitances, it can be noticed that this is not the case for the values of the electric components assigned to the inner porous structure of the cathode. Large average values of $3.10^{18} \Omega$ for R_{Pin} and $5 \text{ F}\cdot\text{s}^{(\alpha-1)}$ for CPE_{in} , far from physical reality, can reflect the difficult step for oxygen passing from the ambient air (gas phase) to dissolved molecules (liquid phase) submitted to diffusion in the porous layer towards the carbon electrode.

Table 4: Impedance parameters fitted as electrical equivalent circuits of Figure 6 on the experimental data for the eight combinations of physicochemical factors as listed in Table 1. Three values (in bold cases) were considered as anomalous and were replaced by the average value of the series.

| | combination | 1 | 2 | 3 | 4 | 5 | 6 | 7 | 8 | mean |
|---------|-----------------------------------|-------------|------|-------------|------|------|------|------|------|------|
| Anode | $R_{ohm} (\Omega)$ | 10.5 | 12.4 | 13.7 | 13.0 | 8.7 | 13.4 | 22.3 | 9.8 | 12.9 |
| | $CPE_{BFads} (mF.s^{(\alpha-1)})$ | 0.41 | 8.37 | 7.14 | 1.18 | 5.65 | 7.16 | 1.88 | 6.38 | 4.77 |
| | α_{BFads} | 0.41 | 0.36 | 0.37 | 0.36 | 0.39 | 0.37 | 0.39 | 0.40 | 0.38 |
| | $R_{BFads} (\Omega)$ | 46.3 | 42.5 | 38.4 | 35.3 | 32.5 | 42.7 | 37.5 | 32.0 | 38.4 |
| | $CPE_{BFdif} (mF.s^{(\alpha-1)})$ | 2.04 | 0.13 | 0.10 | 1.49 | 0.14 | 0.53 | 2.34 | 0.39 | 0.90 |
| | α_{BFdif} | 0.57 | 0.48 | 0.51 | 0.56 | 0.46 | 0.53 | 0.53 | 0.46 | 0.51 |
| | $R_{BFcell} (\Omega)$ | 14.6 | 22.1 | 16.3 | 15.5 | 23.7 | 15.8 | 10.0 | 14.3 | 16.5 |
| | $CPE_{DL} (mF.s^{(\alpha-1)})$ | 2.78 | 3.07 | 2.90 | 2.79 | 3.05 | 3.01 | 3.00 | 3.14 | 2.97 |
| | α_{DL} | 0.86 | 0.88 | 0.88 | 0.84 | 0.87 | 0.87 | 0.85 | 0.87 | 0.86 |
| | $R_p (k\Omega)$ | 10.0 | 12.2 | 10.3 | 6.8 | 11.6 | 11.3 | 11.7 | 10.2 | 10.5 |
| Cathode | $R_{ohm+mem} (\Omega)$ | 27.3 | 13.7 | 13.8 | 21.8 | 10.7 | 18.2 | 17.5 | 11.7 | 16.8 |
| | $CPE_{out} (mF.s^{(\alpha-1)})$ | 1.08 | 1.06 | 1.11 | 1.04 | 1.14 | 1.07 | 1.06 | 1.14 | 1.09 |
| | α_{out} | 0.73 | 0.75 | 0.71 | 0.72 | 0.72 | 0.73 | 0.74 | 0.73 | 0.73 |
| | $R_{Pout} (\Omega)$ | 1428 | 1339 | 1270 | 1285 | 596 | 648 | 594 | 578 | 967 |
| | $CPE_{in} (F.s^{(\alpha-1)})$ | 3.11 | 7.15 | 3.75 | 2.96 | 6.70 | 5.98 | 5.83 | 5.69 | 5.15 |
| | α_{in} | 0.56 | 0.58 | 0.61 | 0.55 | 0.67 | 0.66 | 0.65 | 0.64 | 0.61 |
| | $R_{Pin} (10^{18}\Omega)$ | 3.11 | 1.04 | 3.11 | 3.89 | 2.65 | 2.83 | 4.97 | 3.25 | 3.11 |
| Cell | $CPE_{AN-Th} (mF.s^{(\alpha-1)})$ | 1.82 | 1.22 | 1.33 | 1.08 | 1.40 | 1.19 | 1.29 | 1.49 | 1.35 |
| | α_{AN-Th} | 0.61 | 0.63 | 0.60 | 0.63 | 0.60 | 0.62 | 0.62 | 0.60 | 0.61 |
| | $R_{AN-Th} (\Omega)$ | 3929 | 1719 | 1483 | 1830 | 795 | 737 | 670 | 702 | 1483 |
| | $R_{ohm+mem} (\Omega)$ | 49.6 | 31.4 | 25.0 | 51.1 | 27.9 | 45.7 | 52.1 | 25.3 | 38.5 |
| | $CPE_{K-Th} (mF.s^{(\alpha-1)})$ | 0.94 | 2.47 | 1.07 | 2.56 | 2.59 | 2.41 | 2.36 | 2.55 | 2.12 |
| | α_{K-Th} | 0.67 | 0.92 | 0.64 | 0.93 | 0.88 | 0.86 | 0.88 | 0.89 | 0.83 |
| | $R_{K-Th} (k\Omega)$ | 35.5 | 14.3 | 16.7 | 16.3 | 14.1 | 9.5 | 28.8 | 14.9 | 18.8 |

Table 5 lists the significant (>5 %) relative effects, to their respective mean value, of the experimental factors on the electrical parameters. Unsurprisingly, the most sensitive factor on the series resistances is the conductivity of the solution, directly linked to ionic transport kinetics. A doubling of the conductivity decreases the series resistance by 30 % for the sole electrolyte and 50-60 % when the membrane is taken into account. This is not so clear for the effects of other factors, including the temperature.

Considering the anode and the biofilm characteristics (BF), it can be seen in Table 4 that the α_{BF} average parameters were rather low (0.38 and 0.51), showing that the considered capacitances are far from the ideal capacitive behaviour ($\alpha=1$), possibly due to the living nature of the film and, as previously anticipated, due to the heterogeneities brought by adsorption phenomena. No real trend for the biofilm can be securely extracted from the tables, although some changes are important, like the pseudo-capacitances CPE_{BFads} and CPE_{BFdif} do with conductivity, but in opposite sides. It is however surprising that

temperature is not seen as an important factor able to play a clear positive role on this specific electrical behaviour. In that case of the microbial film, a specific study on the biofilm-on-anode impedance would be valuable to be conducted, including in the early stages of the growing, as to better understand such behaviour²⁸.

Table 5: Relative effects of the experimental factors on the values of the electrical parameters (% on the average). In the chosen experimental ranges, the variations were + 10°C for the temperature, and times 2 for the buffer and acetate concentrations and conductivity. Effects lower than 5% are omitted.

| | Δ_T (+ 10 °C) | $\Delta_{[buffer]}$ (x2) | $\Delta_{[acetate]}$ (x2) | Δ_σ (x2) | |
|--------------------|-------------------------|-----------------------------|------------------------------|-------------------------|--|
| Anode (%) | 9.0 | -11.9 | 17.4 | -28.5 | R_{ohm} electrolyte |
| | 20.8 | 21.4 | -21.0 | 88.6 | CPE_{BFads} biofilm - adsorption |
| | - | - | - | - | α_{BFads} |
| | -11.6 | -6.1 | -7.6 | -10.7 | R_{BFads} |
| | -10.1 | -73.7 | 29.1 | -157.5 | CPE_{BFdif} biofilm - diffusion |
| | -7.4 | - | - | -13.9 | α_{BFdif} |
| | -7.1 | 15.6 | 15.6 | 31.0 | R_{BFcell} |
| | 5.6 | - | - | - | CPE_{DL} double layer - polarization |
| | - | - | - | - | α_{DL} |
| 13.1 | -9.5 | - | 11.0 | R_p | |
| Cathode (%) | -27.6 | -8.8 | -10.7 | -52.0 | $R_{ohm+mem}$ electrolyte + membrane |
| | - | - | - | - | CPE_{out} outer porous structure |
| | - | - | - | - | α_{out} |
| | -75.1 | - | - | - | R_{pout} |
| | 35.1 | -11.6 | 20.0 | 26.2 | CPE_{in} inner porous structure |
| | 13.5 | - | - | - | α_{in} |
| 20.6 | - | - | -38.3 | R_{pin} | |
| Cell (%) | - | -15.5 | -15.7 | - | CPE_{AN-Th} anode |
| | - | - | - | - | α_{AN-Th} |
| | -102 | -36.7 | -31 | -41.6 | R_{AN-Th} |
| | - | - | 10.9 | -57.7 | $R_{ohm+mem}$ electrolyte + membrane |
| | 33.9 | - | 35.4 | - | CPE_{K-Th} cathode |
| | 10.9 | - | 16.9 | - | α_{K-Th} |
| | -20.6 | -49.1 | - | -40.1 | R_{K-Th} |

On the contrary, the DL values, 10.5 k Ω for R_p and 2.97 mF.s^(a-1) for CPE_{DL} , with an α_{DL} parameter as high as 0.86, are similar to those found for a graphite felt anode²⁹ and can be considered as a good representation of the double layer charge transfers mechanisms. These electrical characteristics depicting the

double layer behavior seem to be relatively stable and insensitive to the various factors tested.

For the cathode, all factors seem to affect positively the series resistance, especially conductivity by probably decreasing the membrane resistance³⁰. The outer porous structure seems to be insensitive to the tested electrochemical factors, and only a

decrease of the resistance with temperature is seen. This was expected as this part of the cathode does not lie in direct contact with the electrolyte. For the inner porous structure, more sensitive to the electrochemical factors, it would be risky to draw conclusions as no clear tendency is seen. However, one can notice the decrease of the polarization resistance R_{Pin} with the conductivity of the solution, and the negative evolution of the capacitance and the resistance of the inner porous film with temperature. Other physical factors, like for example oxygen partial pressure, could play a role and would be interesting to be selected for a specific study of this part of the cell.

When the whole cell is considered, with its simplified Thévenin electrical equivalent circuit, the global effects of the experimental factors on both electrodes can be more easily depicted, at least for resistances. In fact, the two electrode resistances appear as significantly positively affected by all factors, especially temperature, buffer concentration and conductivity. For the pseudo-capacitances, one had already seen in Table 5 that their nature can be different as their α parameter values are far from each other (0.61 for the anode and 0.83 for the cathode). This is confirming the perturbations brought by the living microbial anodic layer on the electrochemical behaviour, the cathodic behavior remaining more classical.

Conclusions

This research looked at the characterization of a MFC prototype with a RVC anode and an air-cathode under various physicochemical factors. Temperature was carried in the range 15-25 °C, phosphate buffer concentration in the range 4-8 mM, acetate concentration in the range 7.1-14.3 mM and solution conductivity in the range 2.5-5 mS.cm⁻¹. A rapid and simple experimental plan was conducted that revealed that temperature changes as low as ±1 °C have a very significant effect on every MFC electrochemical parameters (electrode potentials, catalytic currents, maximum power and internal resistance), which is a sign of a kinetic limitation of the reactor. This is concluding that temperature is to be strictly controlled when operating a MFC. Electrolyte conductivity has also a positive effect on the internal resistance, thus reactor power, at the level of ±1 mS.cm⁻¹. For their parts, acetate and buffer concentrations are then considered to have nearly no effect in the range tested. Electrochemical Impedance Spectroscopy, rigorously conducted with experimental determination of the parameters, allowed the fitting of electrical equivalent circuit models on anode, cathode and whole cell. Circuits elements were linked to actual electrochemical mechanisms and their evolution with electrochemical factors were discussed. This systematic study can allow helping the further selection of physical and chemical factors for the search of a positive influence on the behaviour and efficiency of Microbial Fuel Cells.

Acknowledgements

X. Dominguez-Benetton acknowledges Mark Orazem for the insightful discussions on the application of the power-law

model for the calculation of the effective capacitance from EIS data.

Notes

^a Laboratoire Optimisation de la Conception et Ingénierie de l'Environnement (LOCIE), UMR CNRS 5271, Université de Savoie, 73376 Le Bourget du Lac, France.

^b Separation and Conversion Technology, Flemish Institute for Technological Research (VITO), Boeretang 200, Mol 2400, Belgium.

^c Present address: Naturamole, ZA du Villaret, 38350 Susville, France.

^d Present address: Technical University of Denmark, Novo Nordisk Foundation Center for Biosustainability, Kogle Alle 6, 2970 Hørsholm, Denmark.

* Corresponding authors: gerard.perrier@univ-savoie.fr, xoch@vito.be

References

- 1 B. E. Logan, *Appl. Microbiol. Biotechnol.*, 2010, **85**, 1665-1671.
- 2 V. B. Oliveira, M. Simoes, L. F. Melo and A. M. F. R. Pinto, *Biochem. Eng. J.*, 2013, **73**, 53-64.
- 3 H. Richter, K. P. Nevin, H. Jia, D. A. Lowy, D. R. Lovley and L. M. Tender, *Energy Environ. Sci.* 2009, **2**, 506-516.
- 4 D. Pocaznoi, B. Erable, M. -L. Delia and A. Bergel, *Energy Environ. Sci.*, 2012, **5**, 5287-5296.
- 5 D. Hadjiev, D. Dimitrov, M. Martinov and O. Sire, *Enzyme Microbial Technol.*, 2007, **40**, 840-848.
- 6 F. Habouzit, G. Gévaudan, J. Hamelin, J. -P. Steyer and N. Bernet, *Bioresour. Technol.*, 2011, **102**, 4054-4060.
- 7 G. S. Lorite, C. M. Rodrigues, A. A. de Souza, C. Kranz, B. Mizaikoff and M. A. Cotta, *J. Colloid Interface Sci.*, 2011, **359**, 289-295.
- 8 X. Sheng, Y. P. Ting and S. O. Pehkonen, *J. Colloid Interface Sci.*, 2008, **321**, 256-264.
- 9 T. H. Pham, P. Aelterman and W. Verstraete. *Trends Biotechnol.*, 2009, **27**, 168-178.
- 10 G. Lepage, F. O. Albernaz, G. Perrier and G. Merlin, *Bioresour. Technol.*, 2012, **124**, 199-207.
- 11 J. M. Friedrich, C. Ponce-de-Leon, G. W. Reade and F. C. Walsh, *J. Electroanal. Chem.*, 2004, **561**, 203-217.
- 12 S. Cheng, H. Liu and B. E. Logan, *Electrochem. Commun.*, 2006, **8**, 489-494.
- 13 D. P. B. T. B. Strik, A. ter Heijne, H. V. M. Hamelers, M. Saakes and C. J. N. Buisman, *ECS Trans.* 2008, **13**, 27-41.
- 14 X. Dominguez-Benetton, S. Sevda, K. Vanbroekhoven and D. Pant, *Chem. Soc. Rev.*, 2012, **41**, 7228-7246.
- 15 M. Urquidi-Macdonald, S. Real and D. D. Macdonald, *Electrochim. Acta*, 1990, **35**, 1559-1566.
- 16 B. A. Boukamp, *Solid State Ionics*, 2004, **169**, 65-73.
- 17 O. Devos, C. Gabrielli and B. Tribollet, *Electrochim. Acta*, 2006, **51**, 1413-1422.
- 18 B. Hirschorn, M. E. Orazem, B. Tribollet, V. Vivier, I. Frateur and M. Musiani, *J. Electrochem. Soc.*, 2010, **157**, C452-C457.
- 19 B. Hirschorn, M. E. Orazem, B. Tribollet, V. Vivier, I. Frateur and M. Musiani, *J. Electrochem. Soc.*, 2010, **157**, C458-C463.
- 20 S. E. Jorgensen, 2nd ed., 1994, Elsevier Science, Amsterdam, the Netherlands.

- 21 A. Gonzalez del Campo, J. Lobato, P. Canizares, M. A. Rodrigo and F. J. Fernandez Morales, *Appl. Energy*, 2013, **101**, 213-217.
- 22 M. Cappadonia, J. W. Erning, S. M. S. Niaki and U. Stimming, *Solid State Ionics*, 1995, **77**, 65-69.
- 23 R. A. Rozendal, H. V. M. Hamelers and C. J. N. Buisman, *Environ. Sci. Technol.*, 2006, **40**, 5206-5211.
- 24 S. C. Popat, D. Ki, B. E. Rittmann and C. I. Torres, *ChemSusChem*, 2012, **5**, 1071-1079.
- 25 C.I. Torres, A. Kato Marcus and B. E. Rittmann, *Biotechnol. Bioeng.*, 2008, **100**, 872-881.
- 26 J. -Y. Nam, H. -W. Kim, K. -H. Lim, H. -S. Shin and B. E. Logan, *Biosens. Bioelectron.*, 2010, **25**, 1155-1159.
- 27 H. Liu, S. Cheng and B. E. Logan, *Environ. Sci. Technol.*, 2005, **39**, 5488-5493.
- 28 T. Kim, J. Kang, J. -H. Lee and J. Yoon, *Water Res.*, 2011, **45**, 4615-4622.
- 29 A. K. Manohar, O. Bretschger, K. H. Nealon and F. Mansfeld, *Bioelectrochemistry*, 2008, **72**, 149-154.
- 30 K. A. Mauritz and R. B. Moore, *Chem. Rev.*, 2004, **104**, 4535-4585.